International Journal of Hydrogen Energy 98 (2025) 25–34

Contents lists available at ScienceDirect

International Journal of Hydrogen Energy

journal homepage: www.elsevier.com/locate/he

First principles investigations of Lithium based hydrides $LiXH_3$(X=Al, Ga, In) for hydrogen storage applications

Muhammad Ahmed [a], Abu Bakar [a,*], Alibek Orynbassar [b], Nurdaulet Shynarbek [b], Muhammad Ateeq Tahir [c], Erik O. Shalenov [d], Awad A. Ibraheem [e]

[a] Centre of Excellence in Solid State Physics, University of the Punjab, Lahore 54000, Pakistan
[b] Department of Pedagogy of Natural Sciences, SDU University, Kaskelen, Kazakhstan
[c] School of Digital Technologies, Narxoz University, Almaty, Kazakhstan
[d] Department of General Physics, Satbayev University, Almaty, 050013, Kazakhstan
[e] Physics Department, Faculty of Science, King Khalid University, P.O. Box 9004, Abha, Saudi Arabia

ARTICLE INFO

Keywords:
Hydrides
Gravimetric hydrogen storage capacity
Thermoelectric properties
First principles study

ABSTRACT

The investigation of hydrogen storage properties of hydride perovskites have been emerged as great research domain in recent times. The current study focuses on the first principles exploration of lithium based hydrides, $LiXH_3$(X=Al, Ga, In), for hydrogen storage and other physical properties. The structural properties of these hydrides show that the lattice constants of $LiAlH_3$, $LiGaH_3$ and $LiInH_3$ are 3.68, 3.74, and 4.09 Å. respectively. The gravimetric hydrogen storage capacity (C_{wt}%) of $LiAlH_3$, $LiGaH_3$ and $LiInH_3$ is 7.57, 3.66 and 2.37%, respectively. The negative formation energy for these compounds show the stability of these hydrides. The electronic band structures and density of states of under study hydride perovskites validate their metallic nature. The complex dielectric constant, reflectivity and absorption coefficient are investigated to reveal optical response of $LiXH_3$(X=Al, Ga, In). The significant thermodynamic parameters like Debye temperature, specific heat capacities, entropy and thermal expansion coefficient under the effect of temperature and pressure are elaborated to determine the thermodynamic stability. For better understanding of thermoelectric characteristics of these compounds, thermoelectric parameters under wide range of temperature are also studied. The excellent gravimetric hydrogen storage capacity and volumetric hydrogen storage density of these hydride perovskites make them promising materials for hydrogen storage applications.

1. Introduction

The world has recorded its highest energy demand in twenty first century [1,2] due to the industrial revolution and unstoppable growth in population [3,4]. This huge demand of energy has posed multiple challenges and threats to the world economies [5]. Many countries of the world are facing imminent energy crisis. The nations are largely relying on fossil fuels to meet the energy requirements but their unbridled use is one of the major causes for climate change and global warming [6,7]. This century has also witnessed surge in global average temperature and extreme climate change events are now frequent than ever [8–10]. To protect our environment, different world forums have been agreed to work collectively for achieving net zero carbon target [11,12]. This huge demand of energy and global warming can be controlled by investigating alternative green, sustainable and renewable energy sources [13]. Recently, renewable and sustainable energy investigation has been emerged as potential research domain [14,15]. Different alternative energy sources such as solar, hydel and wind power are now talk of the town [16,17]. The hydrogen is also one of the promising alternative, renewable and sustainable energy source [18,19]. The hydrogen is the lightest element and it is abundant in the crust of earth [20]. Different studies have shown that hydrogen can be used as fuel in vehicles without causing any pollution or environmental threats [21–23]. Therefore, hydrogen storage materials are now sought after. Due to their unique characteristics the hydride perovskites are being explored for hydrogen storage applications [24]. Many studies have shown the potential of hydride perovskites for hydrogen storage related applications. The significant attributes of hydride perovskites like simple ABX_3 type structure, higher gravimetric hydrogen storage capacities, structural and dynamical stability, favorable kinetic properties and greater volumetric hydrogen storage densities are their prominent physical features [25–28]. In literature, different hydride perovskites have been reported for their potential optical, thermoelectric, thermodynamic and hydrogen storage applications.

* Corresponding author.
E-mail address: abubakar043@gmail.com (A. Bakar).

https://doi.org/10.1016/j.ijhydene.2024.11.409
Received 26 August 2024; Received in revised form 28 October 2024; Accepted 23 November 2024
Available online 6 December 2024
0360-3199/© 2024 Hydrogen Energy Publications LLC. Published by Elsevier Ltd. All rights are reserved, including those for text and data mining, AI training, and similar technologies.

The magnesium based hydride perovskite $NaMgH_3$ was experimentally synthesize by employing ball milling method [29]. To improve the hydrogen storage properties of $NaMgH_3$, silicon doping was introduced by Anna-Lisa Chaudhary and co-workers [30]. The mechanical milling method was employed by Hui Wu and co-workers to synthesize $NaMgH_3$ [31]. The perovskite hydrides $CaXH_3(X = Mn, Fe, Co)$ were investigated by Surucu et al. [32] for hydrogen storage applications. The highest gravimetric hydrogen storage capacity of 3.09% was reported for $CaMnH_3$ among these compounds. Hafiz Hamid and co-workers explored $XSrH_3(X = K, Rb)$ [33] and reported that $KSrH_3$ and $RbSrH_3$ have gravimetric hydrogen storage capacity of 2.33 and 1.71%, respectively. The hydrides $XSrH_3(X = Cs, Fr)$ were investigated using first principles calculations by Ahmed et al. [34]. This study showed that under study compounds are semiconductors. Similarly, the hydride perovskites $KCaH_3$, $LiCaH_3$, $RbCaH_3$, $KSrH_3$, $LiSrH_3$ and $RbSrH_3$ were investigated by employing first principles calculations for hydrogen storage applications [35]. In this study, $LiCaH_3$ is reported to be most significant compound in comparison to others due to its higher gravimetric hydrogen storage capacity of 6.042%. The indium based hydrides $LiInH_3$ and $KInH_3$ were studied by [36] for hydrogen storage properties using first principles calculations. This study highlighted the importance of these hydrides for their potential use in hydrogen storage applications. Liu [37] and co-workers have introduced the doping of Ni/C nanoparticles to improve the hydrogen storage capacity of $LiAlH_4$. In this way, they reported the 10.5% hydrogen storage capacity of $LiAlH_4$. A first principles study on hydrogen storage properties of Na_2BeH_4 and Na_2MgH_4 reported that these compounds have gravimetric hydrogen storage capacity of 6.78 and 5.38%, respectively [38]. Similarly, the comprehensive theoretical studies on $LiMgF_3$ [39], Na_2CaH_4 [40], $XCuH_3(X = Li, Na, K)$ [41] and $LiAlH_3(A = Mn, Fe, Co)$ [42] have been reported in the literature for hydrogen storage applications using first principles calculations have been reported. This work focuses on the exploration of hydrides $LiXH_3(X = Al, Ga, In)$ for structural, electronic, optical, thermodynamic, thermoelectric and hydrogen storage properties. The high gravimetric hydrogen storage capacity of lithium based hydride perovskites have motivated us to perform first principles calculations based on Density Functional Theory (DFT) to study hydrogen storage and other physical properties $LiXH_3(X = Al, Ga, In)$. The gravimetric hydrogen storage capacity and volumetric hydrogen storage density of novel $LiAlH_3$, $LiInH_3$ and $LiGaH_3$ hydride perovskites have been calculated and the results have been analyzed for their potential utilization in hydrogen storage applications. We have also compare our results with the previous studies in which $LiInH_3$ and $LiAlH_4$ are explored for hydrogen storage applications [36,37,43].

2. Computational details

The Quantum ESPRESSO code [44] has been utilized to carry out first principles calculations based on Density Functional Theory (DFT) by employing Martins and Troullier [45] pseudopotential. The Broyden–Fletcher–Goldfarb–Shanno (BFGS) quasi Newton algorithm [46] is used to perform structural optimization. We have executed comprehensive convergence test to select k-points grid and kinetic cut off energy for these calculations. The Generalized Gradient Approximation of Perdew–Burke–Ernzerhof (PBE-GGA) approach is implemented for exchange and correlation energy [47]. The k-point grid of 8 × 8 × 8 [48] and cut off kinetic energy of 50Ry is used for further calculations. For investigating thermodynamic properties, the quantum quasi harmonic approximation based in Gibbs2 code [49] is employed. The BoltzTraP code integrated with Quantum ESPRESSO based on Boltzmann transport phenomenon is used to determine the thermoelectric properties of these hydrides under wide range of temperature.

Table 1
The lattice constant, volume, bulk modulus, pressure derivative of bulk modulus and formation energy for $LiXH_3(X = Al, Ga, In)$.

Material	a (Å)	$V_0(Å)^3$	B_0(GPa)	B′	E_{form}(eV/atom)
$LiAlH_3$	3.68	49.94	37.3	3.29	−0.927
$LiGaH_3$	3.74	52.61	44.1	3.54	−1.064
$LiInH_3$	4.09	68.53	35.1	4.04	−0.859

3. Results and discussions

3.1. Structural properties

The metallic hydrides $LiXH_3(X = Al, Ga, In)$ show simple cubic structure with in the space group $Pm\bar{3}m$ (No. 221). The lithium (Li) atom is positioned at (0, 0, 0), while X atom (Al, Ga and In) and three Hydrogen atoms are located at (1/2, 1/2, 1/2) and (1/2, 1/2, 0), (1/2, 0, 1/2) and (0, 1/2, 1/2). The optimized lattice constants for each hydride are calculated from energy-volume graph depicted in Fig. 1 ,

This optimized lattice constant is further utilized to calculate essential structural parameters of $LiXH_3(X = Al, Ga, In)$. Table 1 shows lattice constant, volume, optimized bulk modulus, pressure derivative and minimum energy for $LiXH_3(X = Al, Ga, In)$. The lattice constants of $LiAlH_3$, $LiGaH_3$ and $LiInH_3$ are 3.68, 3.74, and 4.09 Å. Note that, lattice constant has been increased while we changed atom at X site of these hydrides and moved from Aluminum to Indium. This slight increase in the lattice constant can be conceptualized in terms of the atomic mass difference. The lattice constant of the hydride having more atomic mass is greater and vice versa. Previous studies of related compounds also validating our calculations [36,50–52]. A previous study reported 3.87 Å lattice constant for $LiInH_3$ [36] and 3.74 Å for $LiInH_3$ [43]. We have used a comprehensive denser k grid of 8 × 8 × 8 [48] and cut off energy of 50Ry to calculate the optimized lattice constant of these hydrides in comparison to previous study for $LiInH_3$. Similarly, the volume of unit cell of $LiAlH_3$, $LiGaH_3$ and $LiInH_3$ is 49.94, 52.61 and 68.53 $(Å)^3$, respectively. The hardness of the material is conceptualized in terms of it's bulk modulus. The bulk modulus of the material is it's ability to resist against external compression. These calculations show that the bulk modulus of $LiAlH_3$, $LiGaH_3$ and $LiInH_3$ is 37.3, 44.1 and 35.1 GPa, respectively. Among these three hydrides, the larger bulk modulus of $LiGaH_3$ indicates it's greater strength.

The stability of these compounds is further examined by calculating the formation energy. The formation energy of $LiAlH_3$, $LiGaH_3$ and $LiInH_3$ is −0.927, −1.064 and −0.859 eV/atom, respectively (see Table 1). The negative formation energy revealed by each compound showing the stability of these hydrides.

3.2. Electronic properties

The electronic properties of $LiXH_3(X = Al, Ga, In)$ are investigated using PBE-GGA technique. The calculation of band structures help to predict the metallic, semiconducting or insulating behavior of any material [53,54]. The Fermi energy and band gap of material also provides basis for optical properties [55]. The electronic band structures of hydrides $LiXH_3(X = Al, Ga, In)$ are shown in Figs. 2(a)–2(c). The highest occupied level is represented by the black dotted line which serves a barrier between valence band and conduction band [56,57]. The band structures are explored between −8eV to 7eV. It is evident from the Figs. 2(a)–2(c) that conduction band is overlapping in valence band. This overlapping advocates that under study hydrides are metallic in nature. We have noted that minima of conduction band along M point is shifting for the case of $LiAlH_3$, $LiGaH_3$ and $LiInH_3$. This shifting is resulted due to the atomic mass difference between these hydrides. The total density of states along with the contribution of each atom is also presented in Figs. 2(a)–2(c). The density of states represents the occupation of electrons against energy. The highest peak of total

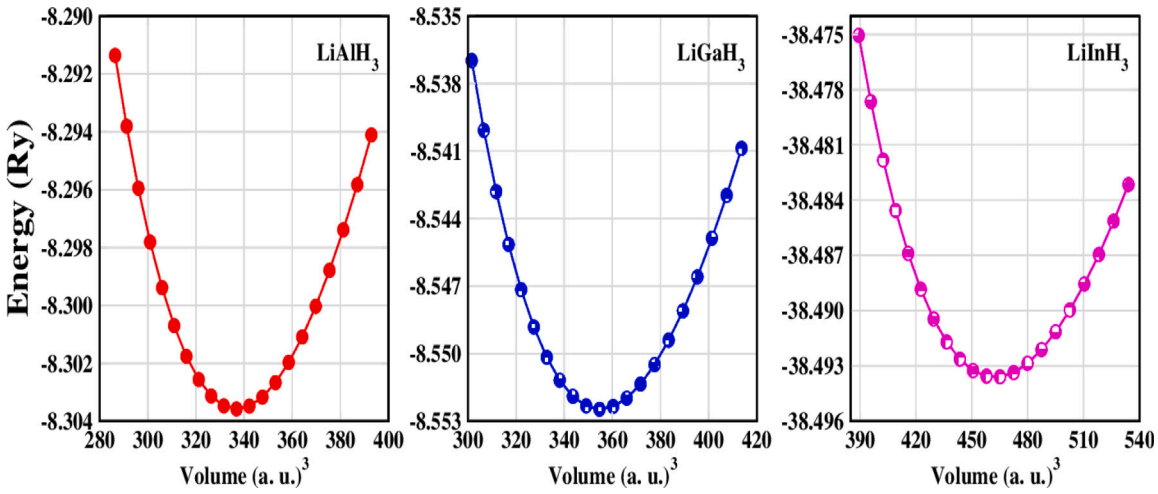


Fig. 1. The energy volume optimization $LiAlH_3$ (red) and $LiGaH_3$ (blue) and $LiInH_3$ (magenta). (For interpretation of the references to color in this figure legend, the reader is referred to the web version of this article.)

density of states in valence band is present at −7eV for $LiAlH_3$. The shifting of this peak towards Fermi level can be viewed for the case of $LiGaH_3$ and $LiInH_3$ in Figs. 2(b) and 2(c). Similarly, different peaks of density of states are present in conduction band indicating the contribution of electrons against specific energy in conduction band. The sharp peaks of density of states present along 2eV to 6eV is arising due to the presence of flattened bands in this energy region.

Table 2
The values of band gap and static optical parameters of $LiXH_3(X = Al, Ga, In)$.

Material	DFT method	E_g(eV)	$\varepsilon(0)$	R(0)
$LiAlH_3$	PBE-GGA	0.00	11.03	0.29
$LiGaH_3$	PBE-GGA	0.00	5.36	0.15
$LiInH_3$	PBE-GGA	0.00	5.79	0.17

3.3. Optical properties

In this section, the optical features of $LiXH_3(X = Al, Ga, In)$ are elucidated. Different optical parameters such as dielectric constant, reflectivity and absorption are explored using PBE-GGA method. The results for these optical parameters are highlighted in Fig. 3 and further assessed for the potential utilization of $LiXH_3(X = Al, Ga, In)$ in optoelectronics industry. The dielectric constant is very essential optical material to investigate the optical response against incoming electromagnetic radiation [58,59]. It can be represented in terms of real and imaginary part using the following mathematical relation [60,61].

$$\varepsilon(\omega) = \varepsilon_1(\omega) + i\varepsilon_2(\omega) \quad (1)$$

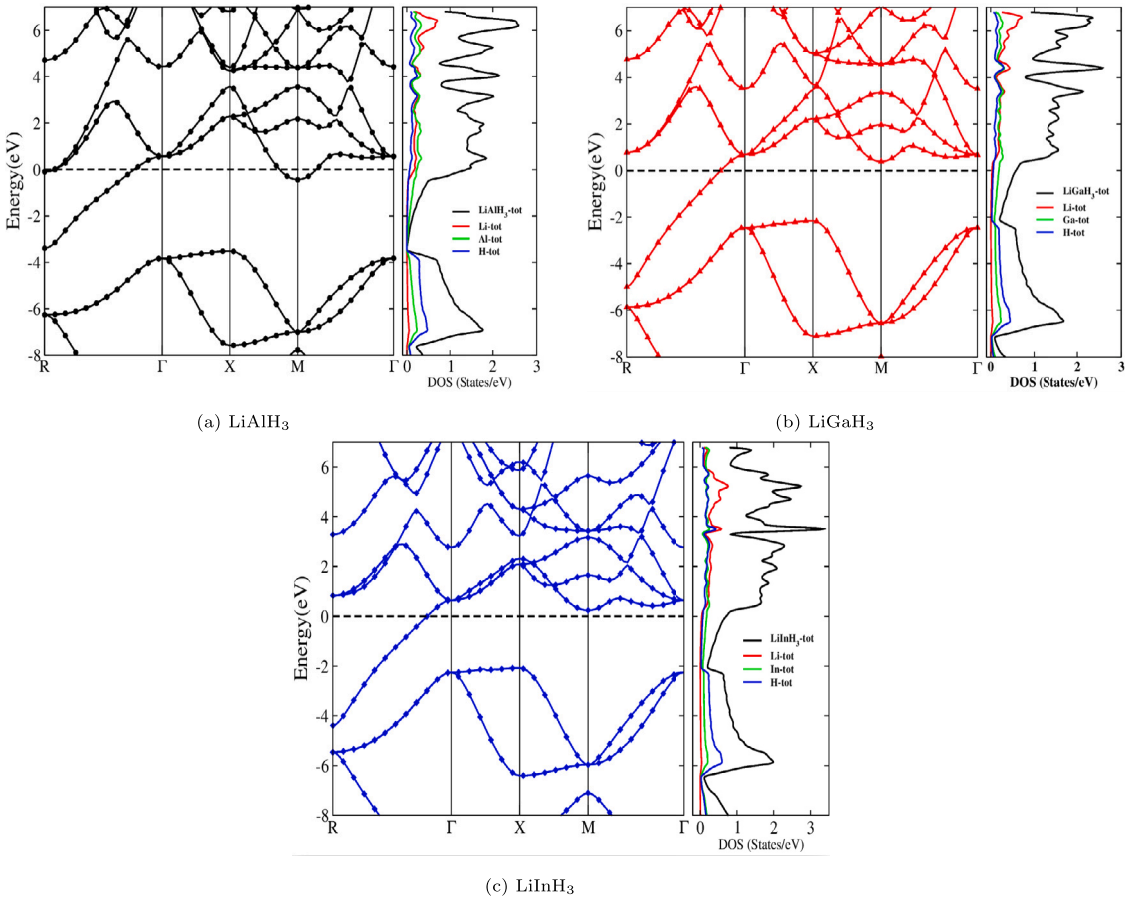
The real and imaginary parts of dielectric constant $\varepsilon(\omega)$ are calculated by employing Kramer's-Kroning relations [62,63].

$$\varepsilon_1(\omega) = 1 + \frac{2}{\pi}\int_0^{\infty} \frac{\omega'\varepsilon_2(\omega)}{\omega'^2 - \omega^2} d\omega' \quad (2)$$

The real part of dielectric constant $\varepsilon_1(\omega)$ for $LiXH_3(X = Al, Ga, In)$ is shown in Fig. 3(a). The applied electromagnetic field give rise to polarization which can be studied in terms of $\varepsilon_1(\omega)$ [64]. The static dielectric constant $\varepsilon(0)$ for $LiAlH_3$, $LiGaH_3$ and $LiInH_3$ is 11.03, 5.36 and 5.80, respectively. The peak values of real part of dielectric constant for $LiAlH_3$ is observed in lower side of visible energy region. While the sharp peaks of $\varepsilon_1(\omega)$ for $LiGaH_3$ and $LiInH_3$ are recorded on shorter wavelength limit of visible region. The spectra of $\varepsilon_1(\omega)$ declines sharply beyond 1eV and remains positive till 6.8 eV. After this value, $\varepsilon_1(\omega)$ becomes negative. Initially, $\varepsilon_1(\omega)$ increases slightly with increasing electromagnetic field and maximum peaks are observed around 3eV. The real part of dielectric constant falls significantly in near ultraviolet energy region for $LiGaH_3$ and $LiInH_3$ and it becomes negative between 4eV to 5eV. The negative spectra of $\varepsilon_1(\omega)$ at any frequency quantifies the strong metallic nature of material and shows the highly reflective behavior [65,66]. The imaginary part of dielectric constant, $\varepsilon_2(\omega)$ for these hydrides is illustrated in Fig. 3(b). The absorption of incident electromagnetic radiation is studied by understanding the spectra of $\varepsilon_2(\omega)$ [67,68]. It starts to increase slowly with increasing energy and the sharp peaks of $LiGaH_3$ and $LiInH_3$ are recorded between 3eV to 5eV. Fig. 3(c) represents the absorption coefficient in response to incoming light for under study hydrides. The absorption of photonic energy in visible region is not significant and peaks start to appear beyond 3eV. The maximum absorption of incident energy is observed between 7eV to 9eV. It shows that these compounds can be utilized for different optoelectronic applications due to the strong absorption at this energy region. The characteristics of a material to reflect back incoming energy is stipulated by reflection coefficient [69,70] which is shown for $LiAlH_3$, $LiGaH_3$ and $LiInH_3$ in Fig. 3. The zero frequency values of dielectric constant and reflectivity for $LiXH_3(X = Al, Ga, In)$ are listed in Table 2. The zero frequency reflectivity offered by $LiAlH_3$, $LiGaH_3$ and $LiInH_3$ is 29%, 15% and 17%. The maximum reflectivity offered by $LiInH_3$ in observed around 7.5 eV and the highest reflectivity for $LiAlH_3$ and $LiGaH_3$ is recorded between 8eV to 10eV.

3.4. Thermodynamic properties

Here we have employed, Debye Quasi-Harmonic approximation to explore thermodynamic properties for $LiXH_3(X = Al, Ga, In)$. The thermodynamic parameters are very necessary to study the thermal stability. For comprehensive study of thermodynamic properties, different parameters like entropy, thermal expansion coefficient, Debye temperature and specific heat capacities are investigated by varying pressure (0 and 5 GPa) and temperature (0–800 K). The disorder in the crystal structure against temperature and pressure is studied by analyzing entropy [71]. The variation of entropy under applied temperature and pressure is illustrated in Fig. 4(a). Results show that entropy increases with temperature and decreases with pressure for these hydrides $LiXH_3(X = Al, Ga, In)$. The maximum entropy is recorded for $LiInH_3$, while $LiAlH_3$ shows minimum entropy. It shows that $LiAlH_3$ is thermally more stable in comparison to other two hydrides. Fig. 4(b) represents the results for thermal expansion coefficient against pressure and temperature variation. The thermal expansion coefficient (α) highlights the change in volume of crystal structure under temperature and pressure [72]. Results show that thermal expansion coefficient for these materials exponentially increases with temperature and decreases



(a) $LiAlH_3$ (b) $LiGaH_3$

(c) $LiInH_3$

Fig. 2. The electronic band structure and density of states of (a) $LiAlH_3$, (b) $LiGaH_3$ and $LiInH_3$. The atomic contributions to the total density of states is also shown.

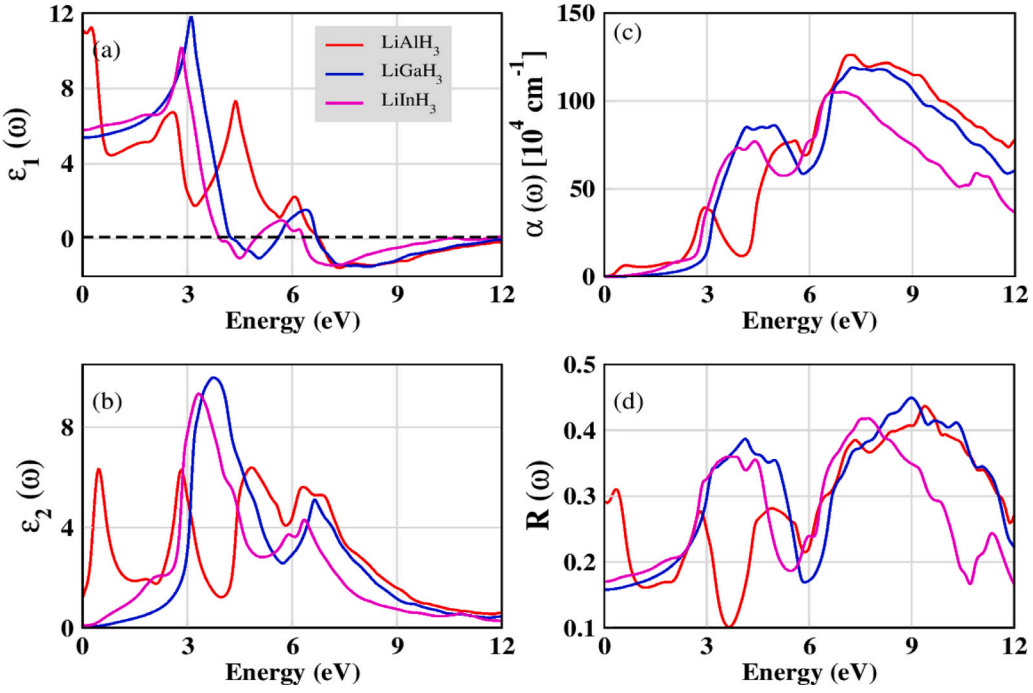


Fig. 3. The complex dielectric constant, absorption coefficient and reflectivity of $LiXH_3$(X = Al, Ga, In) with PBE-GGA and TB-mBJ.

with pressure. At higher temperature side, it is observed that spectra of thermal expansion coefficient becomes parallel to temperature showing the strong absorption of heat. The specific heat capacity at constant volume C_V and specific heat capacity at constant pressure C_P are the amount of energy absorbed per unit mass before temperature change of 1 K. It also varies in the system when temperature and pressure

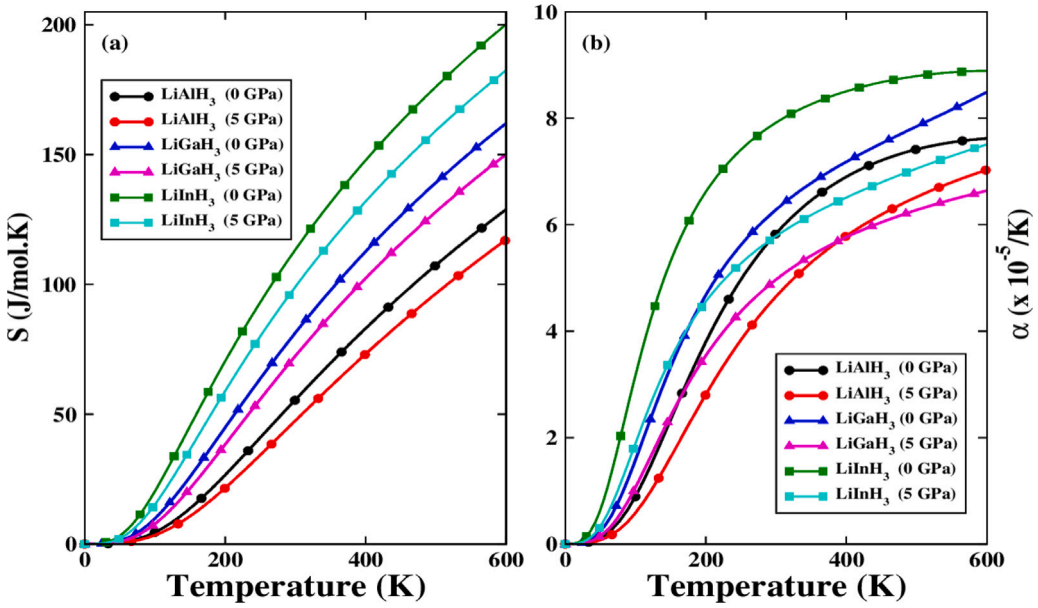


Fig. 4. The variation of entropy (S) and (b) thermal expansion coefficient against temperature and pressure calculated for $LiAlH_3$, $LiGaH_3$ and $LiInH_3$.

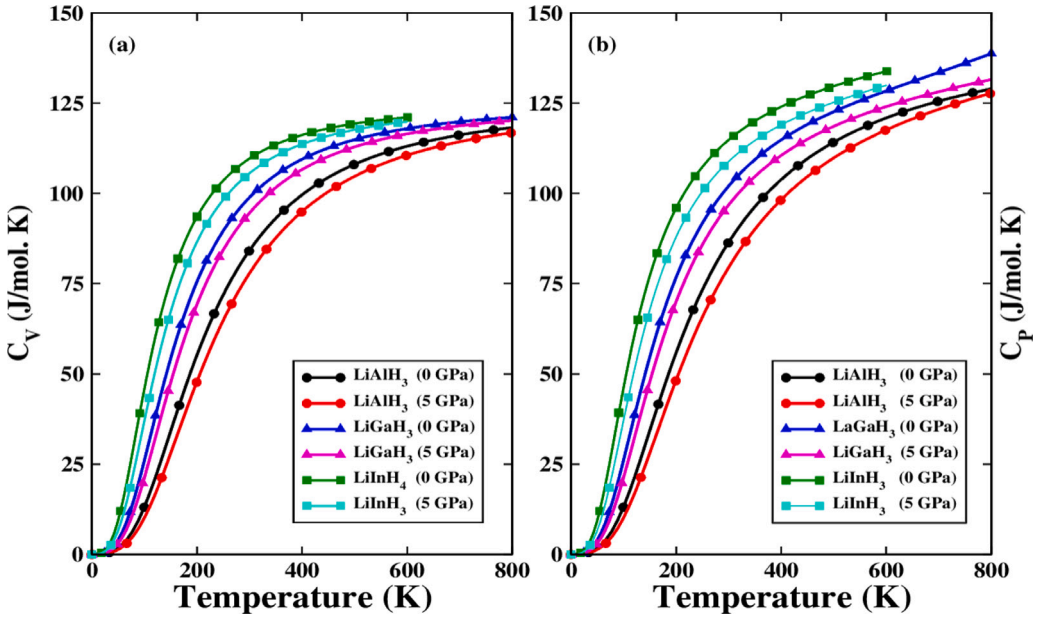


Fig. 5. (a) The variation of specific heat capacity at constant volume, C_V and (b) specific heat capacity at constant pressure, C_P against temperature and pressure calculated for $LiAlH_3$, $LiGaH_3$ and $LiInH_3$.

changes. The spectra of C_V and C_P for $LiXH_3(X = Al, Ga, In)$ is depicted in Fig. 5. The figures show that both C_V and C_P increases with temperature and decreases with pressure. The heat capacities starts to increase significantly with temperature till 200 K. As the temperature increases, the negligible change in the peaks of C_V and C_P is observed and it can be explained on the basis of Debye model of specific heat [73]. The results show that at lower temperature, C_V follows Dulong–Petit law and it becomes almost constant at higher temperature following T^3 law [74]. The Debye temperature Θ_D for $LiXH_3(X = Al, Ga, In)$ against temperature and pressure is plotted in Fig. 6(a). At zero kelvin Θ_D for $LiAlH_3$ is the highest whereas $LiInH_3$ show lowest value among these hydrides. It is also noted that Θ_D increases with pressure as shown by some previous studies related to hydrides. As the temperature increases, Θ_D decreases and approaches to its minimum values at 600 K. The vibrational features of any substance are related to the crucial thermodynamic parameter which is called Grüneisen parameter [75]. It is very important to study the relation between phononic vibrations and harmonic oscillations. The Grüneisen parameter under the effect of temperature and pressure is represented in Fig. 6. The highest value of Grüneisen parameter is recorded for $LiInH_3$ and $LiAlH_3$ possess its minimum value.

3.5. Thermoelectric properties

The growing demand of energy has propelled scientists to investigate novel materials that can convert waste heat into efficient electrical power. The thermoelectric response of material is analyzed by exploring different thermoelectric parameters to check the suitability of material for various applications [76]. In this section, the thermoelectric properties of hydrides $LiXH_3(X = Al, Ga, In)$ are investigated

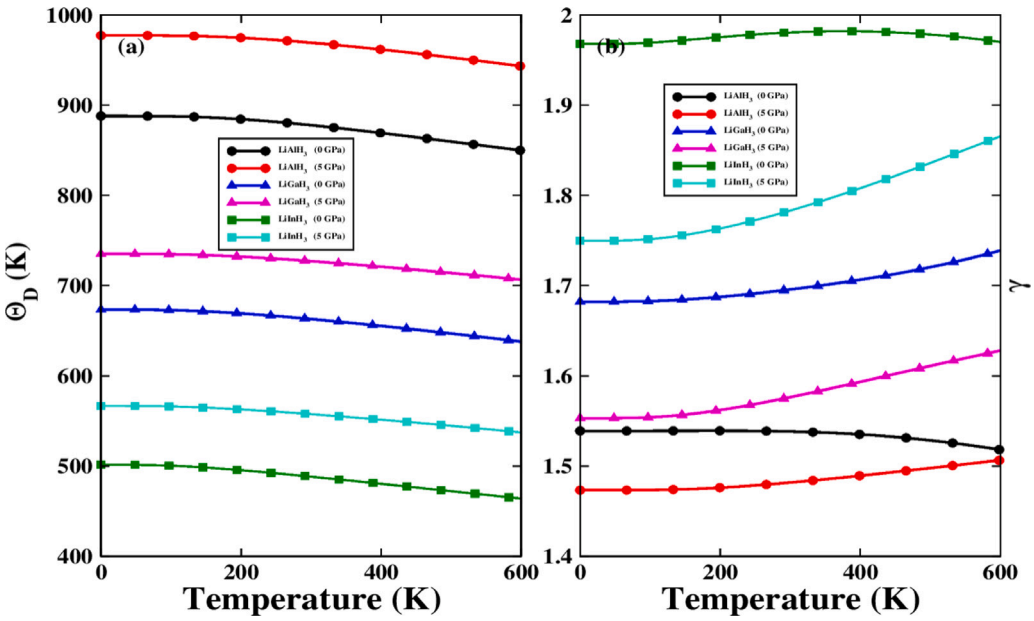


Fig. 6. (a) The variation of (a) Debye temperature and (b) Grüneisen parameter against temperature and pressure calculated for $LiAlH_3$, $LiGaH_3$ and $LiInH_3$.

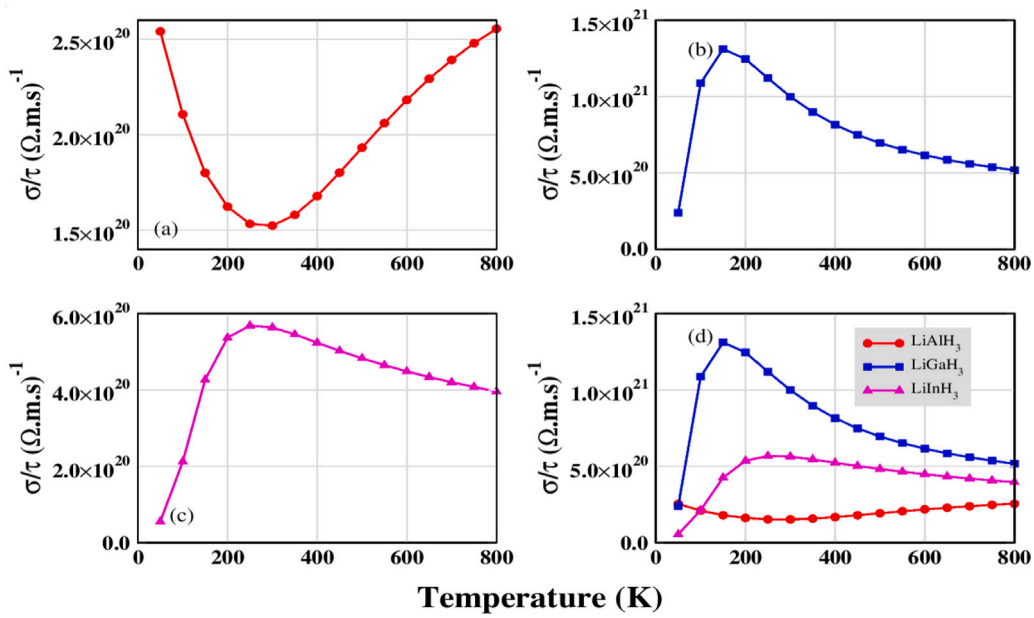


Fig. 7. Electrical conductivity of $LiXH_3(X = Al, Ga, In)$ calculated against temperature.

under a wide range of temperature (0–800 K). The trend of electrical conductivity against temperature for $LiXH_3(X = Al, Ga, In)$ is illustrated in Fig. 7. $LiGaH_3$ exhibit maximum electrical conductivity among these compounds as shown in Fig. 7(b). The electrical conductivity of $LiAlH_3$ starts to decrease first with increasing temperature but after 300 K, it starts to increase indicating the potential of $LiAlH_3$ in thermoelectricity (see Fig. 7(a)). In contrast to this, electrical conductivity of $LiInH_3$ and $LiGaH_3$ first increases with temperature but decreases as we go beyond 300 K (see Fig. 7(b, c)). The comparative analysis show that $LiAlH_3$ shows better response in terms of electrical conductivity with increasing temperature in comparison to other two hydrides. The thermal conductivity for $LiXH_3(X = Al, Ga, In)$ is depicted in Fig. 8. This parameter is usually very essential to analyze the ability of any material for heat sink and thermal insulating applications [77]. The thermal conductivity increases with temperature and it's peak value is observed at 800 K for all three hydrides. We have observed that thermal conductivity of $LiGaH_3$ increases till 100 K and starts to decreases till 300. Beyond this temperature, it again starts to increase with higher temperature as shown in Fig. 8(b). The Seebeck coefficient (S) is the most important thermoelectric parameter which represents the ratio of induced voltage to the change in temperature [78]. The results for Seebeck coefficient are presented in Fig. 9. The Seebeck coefficient varies with temperature as indicated. The Seebeck coefficient for $LiAlH_3$ becomes positive before 200 K and increases till 400 K (see Fig. 9(a)). After this temperature, it starts to decrease gradually till 800 K. A sharp decrease is witnessed for the Seebeck coefficient of $LiGaH_3$ as temperature tends to increase (see Fig. 9(b)). After 200 K, it decreases gradually and approaches to zero at 800 K. For $LiInH_3$, Seebeck coefficient first increases and attains it's maxima and then decreases and becomes zero at 800 K (see Fig. 9(c)). For better view, we have separately plotted Seebeck coefficient for each hydride and then compared the three in Fig (d). The power factor for under study

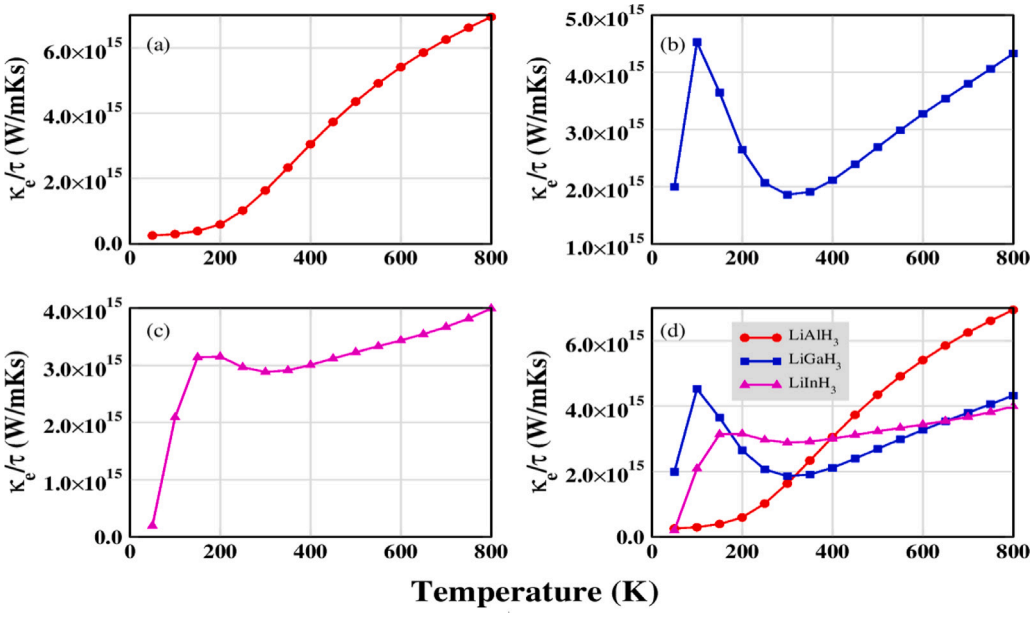


Fig. 8. Thermal conductivity of $LiXH_3(X = Al, Ga, In)$ calculated against temperature.

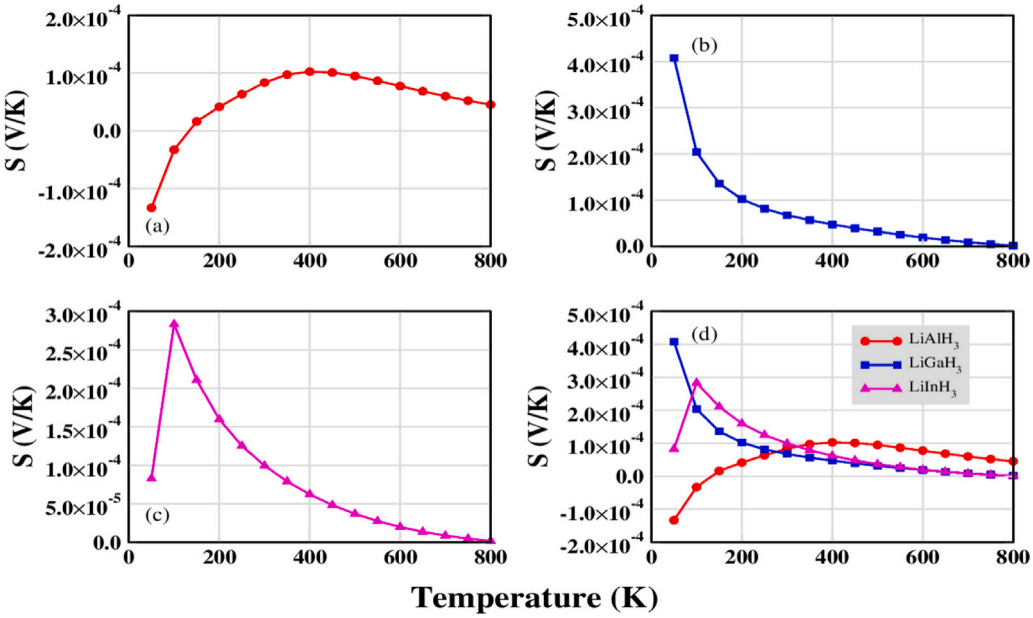


Fig. 9. Seebeck coefficient of $LiXH_3(X = Al, Ga, In)$ calculated against temperature.

hydrides is plotted in Fig. 10. It is observed that power factor for $LiAlH_3$ first decreases and again increases till 450 K. After this temperature, it decreases with increasing temperature (see Fig. 10). After certain temperature, the power factor for $LiGaH_3$ and $LiInH_3$ decreases as shown in Fig. 10(b, c). The figure of merit for under study materials is shown in Fig. 11. At lower temperatures, we obtained good results of figure of merit for these hydrides. But beyond 300 K, figure of merit decreases with increasing temperature (see Fig. 11(a–d)).

3.6. Hydrogen storage properties

The utilization of hydrogen as a fuel is quite challenging due to the unavailability of the potential materials that offer high gravimetric storage capacity, C_{wt}%. The higher gravimetric and volumetric hydrogen storage densities are very important for the synthesis of a material which can be further utilized in hydrogen storage applications. Here, we have computed the gravimetric and volumetric hydrogen storage capacities of hydrides $LiAlH_3$, $LiGaH_3$ and $LiInH_3$. For this purpose, the molar mass of host material and molar mass of hydrogen are used and following mathematical relation is employed to calculate C_{wt}% [79].

$$C_{wt}\% = \frac{(H/M)m_H}{m_{host} + (H/M)m_H} \times 100 \quad (3)$$

Here H/M is the ratio of number of hydrogen atoms to the host atoms, m_H and m_{host} are the molar mass of hydrogen and molar mass of host material. The gravimetric hydrogen storage capacity for hydrides $LiAlH_3$, $LiGaH_3$ and $LiInH_3$ is 7.57, 3.66 and 2.37%, respectively (see Table 3). It has been noticed that C_{wt}% decreases from $LiAlH_3$ to $LiInH_3$. This varying trend is due to the molar mass difference between Al, In and Ga. Among these hydrides, $LiAlH_3$ is the most efficient material due to its significant gravimetric hydrogen storage capacity of 7.57%. The hydrogen storage capacity of $LiAlH_3$

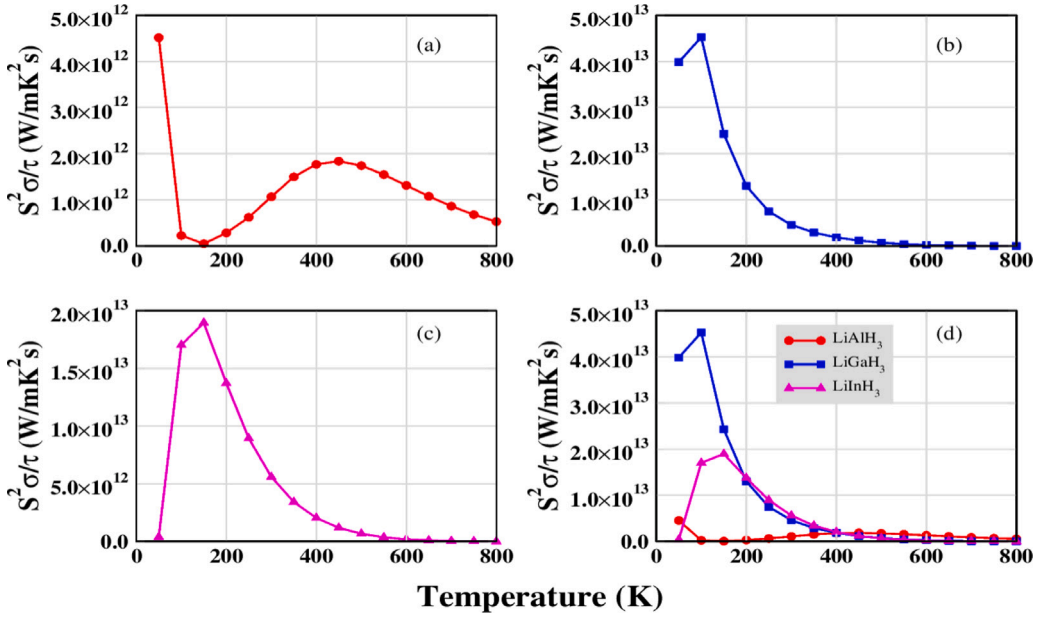


Fig. 10. The power factor of $LiXH_3(X = Al, Ga, In)$ calculated against temperature.

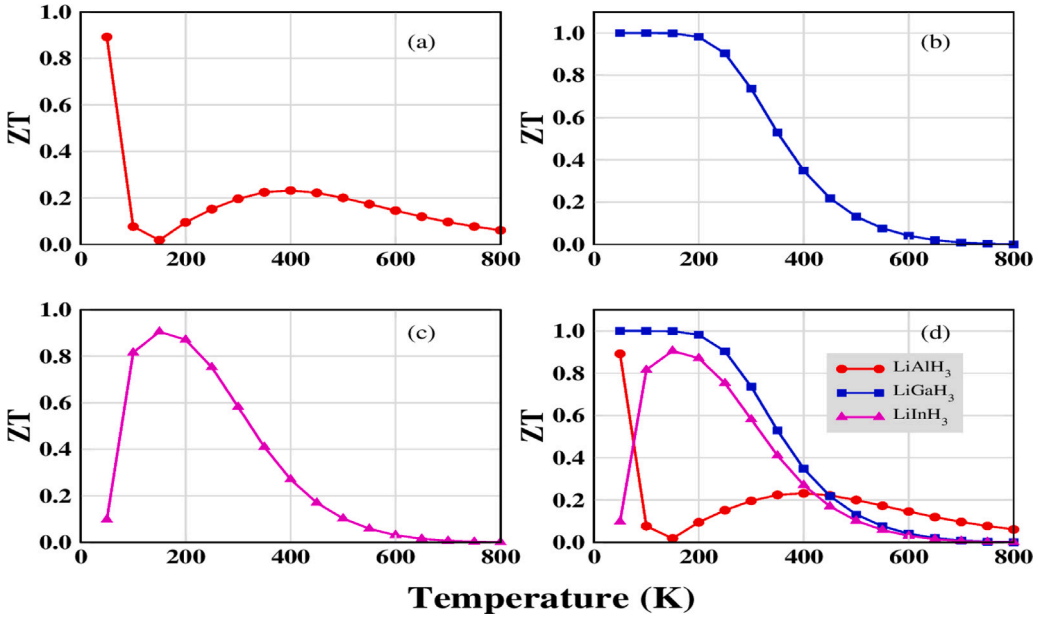


Fig. 11. The figure of merit of $LiXH_3(X = Al, Ga, In)$ calculated against temperature.

Table 3
The hydrogen storage properties, C_{wt}%, ρ_{vol} and desorption temperature, T_d for $LiXH_3(X = Al, Ga, In)$.

Material	C_{wt}%	Other	ρ_{vol}(g.H_2/L)	Other	T_d (K)	Other
$LiAlH_3$	7.57	–	100.55	–	684.374	–
$LiAlH_4$	–	10.5 [37]	–	–	–	–
$LiGaH_3$	3.66	1.86 [43]	95.44	–	785.516	–
$LiInH_3$	2.37	2.42 [36]	73.27	–	634.245	–

is superior than other two compounds which indicates that $LiAlH_3$ can be very efficient material for hydrogen storage applications. The C_{wt}% offered by $LiAlH_3$ is also higher than some previously reported hydrides for hydrogen storage applications such as $KCaH_3$, $KSrH_3$ [80], $XAlH_3(X = K, Rb, Cs)$ [81], $XRuH_3(X = Cr, V, Ni)$ [82], $AVeH_3$ $(X = Be, Mg, Ca, Sr)$ [83]. Additionally, in comparison to previously reported 1.86% hydrogen storage capacity for $LiGaH_3$ [43], our calculations show better results of hydrogen storage capacity of this compound. The volumetric hydrogen storage capacity, ρ_{vol}, is also explored for $LiAlH_3$, $LiGaH_3$ and $LiInH_3$ using given formula [84].

$$\rho_{vol} = \frac{N_H \times m_H}{V(L) \times N_A} \tag{4}$$

In this mathematical relation, N_A represents Avogadro's number, N_H shows the number of hydrogen atoms and $V(L)$ is the volume of unit cell. Table 3 shows the calculated values of ρ_{vol} for under study hydrides. $LiAlH_3$, $LiGaH_3$ and $LiInH_3$ have the volumetric hydrogen storage of 100.55, 95.44 and 73.27 g.H_2/L, respectively. Similar to the results of C_{wt}%, $LiAlH_3$ exhibits largest value of ρ_{vol} in comparison to $LiGaH_3$ and $LiInH_3$. The desorption temperature of the hydrides can be calculated using following expression [42,85].

$$T_d = \frac{-\Delta H_f}{\Delta S} \tag{5}$$

The desorption temperature for these hydrides has been calculated and listed in Table 3.

4. Conclusion

This work focuses on hydrogen storage and other physical properties of novel lithium based hydride perovskites $LiXH_3(X = Al, Ga, In)$ using Density Functional Theory (DFT). The optimized structural parameters like lattice constant, optimized volume, optimized bulk modulus and total energy are first calculated. The gravimetric hydrogen storage capacity (Volumetric hydrogen storage density) of $LiAlH_3$, $LiGaH_3$ and $LiInH_3$ is 7.57 (100.55), 3.66 (95.44) and 2.37 (73.27). The electronic properties revealed that these hydrides have zero band gap thus confirming their metallic nature. To elucidate the optical response of these hydrides, different optical parameters are investigated. The static dielectric constant of $LiAlH_3$, $LiGaH_3$ and $LiInH_3$ is 11.03, 5.36 and 5.79, respectively. The effect of pressure and temperature on thermodynamic parameters is analyzed comprehensively. The analysis show that entropy and thermal expansion coefficient of under study compounds increases with temperature and decreases with pressure. The thermoelectric properties of $LiAlH_3$, $LiGaH_3$ and $LiInH_3$ are also explored. The comparative analysis indicates that power factor of $LiAlH_3$ increases significantly with increasing temperature. The high gravimetric hydrogen storage capacity and volumetric hydrogen storage density of $LiAlH_3$ in comparison to $LiGaH_3$ and $LiInH_3$ anticipates its great potential for hydrogen storage applications.

CRediT authorship contribution statement

Muhammad Ahmed: Writing – original draft, Visualization, Investigation, Conceptualization. **Abu Bakar:** Writing – review & editing, Writing – original draft, Supervision, Software, Resources, Investigation, Formal analysis, Data curation, Conceptualization. **Alibek Orynbassar:** Writing – original draft, Investigation, Formal analysis. **Nurdaulet Shynarbek:** Validation, Investigation, Data curation. **Muhammad Ateeq Tahir:** Visualization, Investigation, Formal analysis. **Erik O. Shalenov:** Writing – original draft, Validation, Methodology, Conceptualization. **Awad A. Ibraheem:** Writing – original draft, Validation, Formal analysis, Conceptualization.

Declaration of competing interest

The authors declare that they have no known competing financial interests or personal relationships that could have appeared to influence the work reported in this paper.

Acknowledgments

The authors extend their appreciation to Deanship of Scientific Research at King Khalid University for funding this research work through large groups project under grant number R.G.P.2/89/45.

Data availability

Data will be made available on reasonable request.

References

[1] MacKenzie JJ. Energy and environment in the 21st century: The challenge of change. In: Energy and environment. Routledge; 2021, p. 15–47.
[2] Fanchi JR. Energy in the 21st century: Energy in transition. World Scientific; 2023.
[3] Coyle ED, Simmons RA. Understanding the global energy crisis. Purdue University Press; 2014.
[4] Warner KJ, Jones GA. The climate-independent need for renewable energy in the 21st century. Energies 2017;10(8):1197.
[5] Armaroli N, Balzani V. The future of energy supply: challenges and opportunities. Angew Chem, Int Ed Engl 2007;46(1–2):52–66.
[6] Abas N, Kalair A, Khan N. Review of fossil fuels and future energy technologies. Futures 2015;69:31–49.
[7] Dorian JP, Franssen HT, Simbeck DR. Global challenges in energy. Energy policy 2006;34(15):1984–91.
[8] Huber D, Gulledge J. Extreme weather and climate change. 2011, Center for Climate and Energy Solutions.
[9] Rahmstorf S, Coumou D. Increase of extreme events in a warming world. Proc Natl Acad Sci 2011;108(44):17905–9.
[10] Luber G, McGeehin M. Climate change and extreme heat events. Am J Prevent Med 2008;35(5):429–35.
[11] Fankhauser S, Smith SM, Allen M, Axelsson K, Hale T, Hepburn C, Kendall JM, Khosla R, Lezaun J, Mitchell-Larson E, et al. The meaning of net zero and how to get it right. Nature Clim Change 2022;12(1):15–21.
[12] Deutch J. Is net zero carbon 2050 possible? Joule 2020;4(11):2237–40.
[13] Ali M, Munir J, Khan MJI, Yousaf M, Younis M, Saeed M. CO Adsorption on two-dimensional 2H-ZrO2 and its effect on the interfacial electronic properties: implications for sensing. Phys Scr 2023;98(11):115801.
[14] Hussain A, Arif SM, Aslam M. Emerging renewable and sustainable energy technologies: State of the art. Renew Sustain Energy Rev 2017;71:12–28.
[15] Ali M, Bibi Z, Younis M, Mubashir M, Iqbal M, Ali MU, Iqbal MA. An accurate prediction of electronic structure, mechanical stability and optical response of BaCuF3 fluoroperovskite for solar cell application. Sol Energy 2024;267:112199.
[16] Barbosa LdNS, Bogdanov D, Vainikka P, Breyer C. Hydro, wind and solar power as a base for a 100% renewable energy supply for South and Central America. PLoS One 2017;12(3):e0173820.
[17] Rahman A, Farrok O, Haque MM. Environmental impact of renewable energy source based electrical power plants: Solar, wind, hydroelectric, biomass, geothermal, tidal, ocean, and osmotic. Renew Sustain Energy Rev 2022;161:112279.
[18] Hosseini SE, Wahid MA. Hydrogen production from renewable and sustainable energy resources: Promising green energy carrier for clean development. Renew Sustain Energy Rev 2016;57:850–66.
[19] Abbasi T, Abbasi S. 'Renewable'hydrogen: prospects and challenges. Renew Sustain Energy Rev 2011;15(6):3034–40.
[20] Zohuri B, Zohuri B. The chemical element hydrogen. In: Hydrogen energy: challenges and solutions for a cleaner future. Springer; 2019, p. 1–35.
[21] Fayaz H, Saidur R, Razali N, Anuar FS, Saleman A, Islam M. An overview of hydrogen as a vehicle fuel. Renew Sustain Energy Rev 2012;16(8):5511–28.
[22] Jain IP. Hydrogen the fuel for 21st century. Int J Hydrog Energy 2009;34(17):7368–78.
[23] Tollefson J, et al. Hydrogen vehicles: fuel of the future. Nature 2010;464(7293):1262–4.
[24] Masood MK, Khan W, Chaoui K, Ashraf Z, Bibi S, Kanwal A, Alothman AA, Rehman J. Theoretical investigation of XSnH3 (X: Rb, Cs, and Fr) perovskite hydrides for hydrogen storage application. Int J Hydrog Energy 2024;63:1248–57.
[25] Orimo S-i, Nakamori Y, Eliseo JR, Züttel A, Jensen CM. Complex hydrides for hydrogen storage. Chem Rev 2007;107(10):4111–32.
[26] Schneemann A, White JL, Kang S, Jeong S, Wan LF, Cho ES, Heo TW, Prendergast D, Urban JJ, Wood BC, et al. Nanostructured metal hydrides for hydrogen storage. Chem Rev 2018;118(22):10775–839.
[27] Schüth F, Bogdanović B, Felderhoff M. Light metal hydrides and complex hydrides for hydrogen storage. Chem Commun 2004;(20):2249–58.
[28] Rusman N, Dahari M. A review on the current progress of metal hydrides material for solid-state hydrogen storage applications. Int J Hydrog Energy 2016;41(28):12108–26.
[29] Tao S, Wang Z-m, Wan Z-z, Deng J-q, Zhou H, Yao Q. Enhancing the dehydriding properties of perovskite-type NaMgH3 by introducing potassium as dopant. Int J Hydrog Energy 2017;42(6):3716–22.
[30] Chaudhary A-L, Paskevicius M, Sheppard DA, Buckley CE. Thermodynamic destabilisation of MgH2 and NaMgH3 using group IV elements Si, Ge or Sn. J Alloys Compd 2015;623:109–16.
[31] Wu H, Zhou W, Udovic TJ, Rush JJ, Yildirim T. Crystal chemistry and dehydrogenation/rehydrogenation properties of perovskite hydrides RbMgH3 and RbCaH3. J Phys Chem C 2009;113(33):15091–8.
[32] Surucu G, Gencer A, Candan A, Gullu HH, Isik M. CaXH3 (X=Mn, Fe, Co) perovskite-type hydrides for hydrogen storage applications. Int J Energy Res 2020;44(3):2345–54.
[33] Raza HH, Murtaza G, Muhammad N, Ramay SM. First-principle investigation of XSrH3 (X=K and Rb) perovskite-type hydrides for hydrogen storage. Int J Quantum Chem 2020;120(24):e26419.
[34] Ahmed M, Fatima R, Bakar A, Orynbassar A, Shynarbek N, Khairy Y. Exploration of hydrides XSrH3 (X=Cs, Fr) for hydrogen storage applications: A first principles study. Int J Hydrog Energy 2024;83:460–71.

[35] Song Y, Shahzad MK, Hussain S, Farrukh A, Riaz M, Sattar H, Khan G, Ashraf GA, Ali SM, Alam M. Theoretical prediction of perovskite ARH3 (A=K, Li, Rb; RCa, Sr) hydride materials for hydrogen storage applications: A DFT investigation. Int J Hydrog Energy 2024;79:1472–82.

[36] Deen SM, Usman M, Rehman JU, Ali SM, Ali M. A DFT study for physical properties and hydrogen storage capability of indium-based hydride perovskites XInH3 (X=Li, K) for hydrogen storage application. Solid State Commun 2024;384:115488.

[37] Liu Z, Liu J, Wei S, Xia Y, Cheng R, Sun L, Xu F, Huang P, Bu Y, Cheng J, et al. Improved hydrogen storage properties and mechanisms of LiAlH4 doped with Ni/C nanoparticles anchored on large-size Ti3C2Tx. J Alloys Compd 2023;931:167353.

[38] Ali M, Bibi Z, Awais M, Younis M, Sfina N. Effective hydrogen storage in Na2 (Be/Mg) H4 hydrides: Perspective from density functional theory. Int J Hydrog Energy 2024;64:329–38.

[39] Mubashir M, Ali M, Bibi Z, Younis M, Muzamil M. Efficient hydrogen storage in LiMgF3: a first principle study. Int J Hydrog Energy 2024;50:774–86.

[40] Ali M, Bibi Z, Younis M, Majeed K, Afzal U, Khan S, Alotaibi NH, Mubashir M. Enhancement of hydrogen storage characteristics of Na2CaH4 hydrides by introducing the Mg and Be dopant: A first-principles study. Int J Hydrog Energy 2024;70:579–90.

[41] Mubashir M, Ali M, Bibi Z, Afzal U, Albaqami MD, Mohammad S, Muzamil M. Computational evaluation of novel XCuH3 (X=Li, Na and K) perovskite-type hydrides for hydrogen storage applications using LDA and GGA approach. J Mol Graph Model 2024;108808.

[42] Ali M, Bibi Z, Mubashir M, Younis M, Afzal U, El-marghany A. A computational investigation of lithium-based metal hydrides for advanced solid-state hydrogen storage. ChemistrySelect 2024;9(10):e202304582.

[43] Usman M, ur Rehman J, Tahir MB, Hussain A. Structural, electronics, magnetic, optical, mechanical and hydrogen storage properties of Ga-based hydride-perovskites X GaH3 (X=K, Li). Int J Energy Res 2022;46(11):15617–26.

[44] Giannozzi P, Andreussi O, Brumme T, Bunau O, Nardelli MB, Calandra M, Car R, Cavazzoni C, Ceresoli D, Cococcioni M, et al. Advanced capabilities for materials modelling with Quantum ESPRESSO. J Phys: Condensed Matter 2017;29(46):465901.

[45] Troullier N, Martins JL. Efficient pseudopotentials for plane-wave calculations. Phys Rev B 1991;43(3):1993.

[46] Gill PE, Murray WA, et al. Numerical methods for constrained optimization. 1974.

[47] Perdew JP, Burke K, Ernzerhof M. Generalized gradient approximation made simple. Phys Rev Lett 1996;77(18):3865.

[48] Monkhorst HJ, Pack JD. Special points for Brillouin-zone integrations. Phys Rev B 1976;13:5188–92.

[49] Otero-de-la Roza A, Abbasi-Pérez D, Luaña V. Gibbs2: A new version of the quasiharmonic model code. II. Models for solid-state thermodynamics, features and implementation. Comput Phys Comm 2011;182(10):2232–48.

[50] Ahmed B, Tahir MB, Ali A, Sagir M. First-principles screening of structural, electronic, optical and elastic properties of Cu-based hydrides-perovskites XCuH3 (X=Ca and Sr) for hydrogen storage applications. Int J Hydrog Energy 2024;54:1001–7.

[51] Shah M, Nuruzzaman M, Hossain A, Jubair M, Zilani M. A DFT insight into structural, mechanical, elasto-acoustic, and anisotropic properties of AePdH3 (Ae=Ca, Sr, Ba) perovskites under pressure. Comput Condensed Matter 2023;34:e00774.

[52] Mubashir M, Ali M, Yousaf M, Huang H, Khan MJI. Exploring promising KAH3 (A=Ca, Sr and Ba) hydrides for solid-state hydrogen storage and thermoelectric applications. Int J Hydrog Energy 2024;82:1435–45.

[53] Ahmed M, Bakar A, Quader A, Ahmad RA, Ramay SM. First-principles calculations to investigate structural, elastic, mechanical, electronic and optical characteristics of RbSrX3 (X=Cl, Br). Chem Phys 2024;581:112260.

[54] Younis M, Akhter T, Yousaf M, Ali M, Naeem H. Controlled dynamic variation of interfacial electronic and optical properties of lithium intercalated ZrO2/MoS2 vdW heterostructure. J Mol Graph Model 2024;127:108694.

[55] Yousaf M, Younis M, Jbara AS, Khan MJI, Murtaza G, Saeed M. Effect of layer sliding on the interfacial electronic properties of intercalated silicene/indium selenide van der waals heterostructure. Commun Theor Phys (Beijing) 2022;74(3):035701.

[56] Ahmed M, Bakar A, Tahir MA, Nawaz R, Ibraheem AA. The use of nonlocal corrections and SCAN to compute the electronic, optical and thermoelectric properties of XCuF3 (X=K, Rb). Optik 2024;310:171877.

[57] Younis M, Akhter T, Yousaf M, Munir J, Naeem H, Ali M. Layer-sliding-mediated reversible tuning of interfacial electronic and optical properties of intercalated ZrO2/MoS2 van der waals heterostructure. J Mater Res 2023;38(23):4995–5007.

[58] Ahmed M, Bakar A, Dzhumagulova KN, Quader A, et al. A first-principles investigations of lead-free SbPCa3 inverse perovskite for structural, electronic and optical properties with different DFT methods. Physica B 2024;690:416250.

[59] Mubashir M, Bibi Z, Ali M, Muzamil M, Afzal U, Albaqami MD. First-principles prediction of antimony based XSbF3 (X=Be, Mg, Ca and Sr) fluoroperovskites: An insight into structural, optoelectronic and thermal properties. Physica B 2024;685:415986.

[60] Ahmed M, Bakar A, Ahmad RA, Ramay SM. First-principles investigations for electronic and thermoelectric properties of XGeF3 (X=K, Rb): Nonlocal corrections and SCAN insights. Physica B 2024;688:416114.

[61] Mubashir M, Ali M, Ain Q, Khan MA, Ghaithan HM, Bibi Z, Aldwayyan AS, Ahmed AAA, Qaid SM. First-principles screening of XSbF3 (X=Ba and Ra) fluoroperovskites: an insight into structural, optoelectronic and thermal properties. Phys Scr 2024;99(6):0659b3.

[62] Xiong K, Robertson J, Clark SJ. Behavior of hydrogen in wide band gap oxides. J Appl Phys 2007;102:083710–23. http://dx.doi.org/10.1063/1.2798910.

[63] W. Johnson D. A Fourier series method for numerical Kramers-Kronig analysis. J Phys A Math Gen 1975;8(4):490–5. http://dx.doi.org/10.1088/0305-4470/8/4/009.

[64] Ali M, Yousaf M, Naeem H, Munir J. Layer-sliding-mediated controllable synthetic strategy for the preparation of multifunctional materials. Mater Today Commun 2023;37:107022.

[65] Bakar A, Afaq A, Ahmed M, Bashir A, Asif M. Optoelectronic properties of CuCoMnZ (Z=Si, Sn, Sb): A DFT study. J Electron Mater 2021;50(7):4006–15.

[66] Ali M, Yousaf M, Munir J, Khan MJI, ul Ain Q, Younis M. Controlled dynamic variation of interfacial electronic and optical properties of sodium-intercalated silicene/hBN heterostructure. Eur Phys J Plus 2023;138(12):1151.

[67] Pingak RK, Ngara ZS, Johannes AZ, Bukit M, Tanesib JL. Novel KXBr3 (X=Ca, Sr, Ba) lead-free halide perovskites for optoelectronic applications: A DFT investigation of mechanical and optoelectronic properties. Computational Condensed Matter 2024;e00928.

[68] Ali M, Yousaf M, Munir J, et al. Achieving controllable multifunctionality through layer sliding. J Mol Graph Model 2024;126:108638.

[69] Hosen A, Hossain MA, Abu-Jafar MS, Pingak RK, Mousa AA. Unraveling Lead-Free Fr-Based Perovskites FrQCl3 (Q=Ca, Sr) and their pressure induced physical properties: DFT Analysis for Advancing Optoelectronic Performance. J Phys Chem Solids 2024;112211.

[70] Ali M, Bibi Z, Younis M, Iqbal MA. Structural, optoelectronic and thermodynamical insights into 2H-ZrO2: A DFT investigation. Inorg Chem Commun 2024;160:111891.

[71] Ul Aarifeen N, Afaq A. Effects of temperature and pressure on thermodynamic properties of Cd0. 50 Zn0. 50 Se alloy. Mater Res Express 2017;4(9):095901.

[72] Aarifeen Nu, Ahmad A, Munir HB, Bakar A. First principles study of thermodynamic properties of CdxZn1- xO (0⩽ x⩽ 1) ternary alloys. Z Naturforschung A 2019;74(12):1115–22.

[73] Blackman M. The theory of the specific heat of solids. Rep Progr Phys 1941;8(1):11.

[74] Fitzgerel RK, Verhoek FH. The law of Dulong and Petit. ACS Publications; 1960.

[75] Ul Aarifeen N, Afaq A. Theoretical prediction of thermodynamic properties of Cd x Zn 1-x S (0⩽ x⩽ 1) under the effects of pressure (0-10 GPa) and temperature (0-1200 K). Acta Phys Pol: A 2020;137(3).

[76] Asif M, Alrashdi AO, Fadhali MM, Afaq A, Bakar A. First-principles investigations of thermoelectric behavior of RuCrX (X= Si, Ge, Sn). ACS omega 2022;7(49):45353–60.

[77] Afaq A, Akhtar SEA, Bakar A, Ramay SM. Electronic, phonon and thermoelectric properties of MnCrX (X=As, P, Sb) half Heusler alloys: a DFT study. Indian J Phys 2024;1–7.

[78] ul Haq A, Ahmad TS, Amin M, Bakar A, Afaq A, Ehsan N, Ramay SM, Siddig AA. A first principle investigation of electronic, mechanical, optical and transport properties of A2AgAlI6 (A=Rb, K, Na) for energy harvesting. Phys Scr 2023;98(11):115972.

[79] Raza HH, Murtaza G, Shafiq M, Shakoor SA. First-principles calculations on structural, mechanical and thermodynamic properties of orthorhombic Mg2BeTMH8 (TM=Ni, Cu and zn) for hydrogen storage applications. Int J Hydrog Energy 2024;62:637–51.

[80] Kurkcu C, Al S, Yamcicier C. Investigation of mechanical properties of KCaH3 and KSrH3 orthorhombic perovskite hydrides under high pressure for hydrogen storage applications. Eur Phys J B 2022;95(11):180.

[81] Umer M, Murtaza G, Ahmad N, Ayyaz A, Raza HH, Usman A, Liaqat A, Manoharadas S. First principles investigation of structural, mechanical, thermodynamic, and electronic properties of Al-based perovskites XAlH3 (X=K, Rb, Cs) for hydrogen storage. Int J Hydrog Energy 2024;61:820–30.

[82] Parvaiz MM, Khalil A, Tahir MB, Ayub S, Ali TE, Masood HT. A DFT investigation on structural, electronic, magnetic, optical, elastic and hydrogen storage properties of Ru-based hydride-perovskites XRuH 3 (X=Cr, V, Ni). RSC Adv 2024;14(12):8385–96.

[83] Siddique A, Khalil A, Almutairi BS, Tahir MB, Sagir M, Ullah Z, Hannan A, Ali HE, Alrobei H, Alzaid M. Structures and hydrogen storage properties of AeVH3 (Ae=Be, Mg, Ca, Sr) perovskite hydrides by DFT calculations. Int J Hydrog Energy 2023;48(63):24401–11.

[84] Muhammad S, Murtaza G, Azam A, Raza H, Arif Khalil R, Hussain MI, Waqas Iqbal M. Tailoring magnesium-based hydrides as potential and reversible materials for solid-state hydrogen storage: A first-principles study. Internat J Modern Phys B 2024;38(26):2450358.

[85] Ain Q, Naeem HT, Ali M, Munir J, Bibi Z, Ghaithan HM, Ahmed AAA, Qaid SM. A precise prediction of structure stability and hydrogen storage capability of KCdH3 perovskite hydride using density functional theory calculations. J Energy Storage 2024;100:113734.